In-Process Thermal Imaging of the Electron Beam Freeform Fabrication Process

Karen M. Taminger*[a], Christopher S. Domack[b], Joseph N. Zalameda[a],
Brian L. Taminger[b], Robert A. Hafley[a], Eric R. Burke[a]
[a]NASA Langley Research Center, Hampton, VA 23681
[b]Analytical Mechanics Associates, Inc., 21 Enterprise Pkwy., Suite 300, Hampton, VA 23666-6413

ABSTRACT

Researchers at NASA Langley Research Center have been developing the Electron Beam Freeform Fabrication (EBF^3) metal additive manufacturing process for the past 15 years. In this process, an electron beam is used as a heat source to create a small molten pool on a substrate into which wire is fed. The electron beam and wire feed assembly are translated with respect to the substrate to follow a predetermined tool path. This process is repeated in a layer-wise fashion to fabricate metal structural components. In-process imaging has been integrated into the EBF^3 system using a near-infrared (NIR) camera. The images are processed to provide thermal and spatial measurements that have been incorporated into a closed-loop control system to maintain consistent thermal conditions throughout the build. Other information in the thermal images is being used to assess quality in real time by detecting flaws in prior layers of the deposit. NIR camera incorporation into the system has improved the consistency of the deposited material and provides the potential for real-time flaw detection which, ultimately, could lead to the manufacture of better, more reliable components using this additive manufacturing process.

Keywords: Electron beam, additive manufacturing, thermal imaging, near infrared (NIR), short wave infrared (SWIR), image analysis, closed-loop control, nondestructive evaluation

1. INTRODUCTION

For the past 15 years, researchers at the NASA Langley Research Center (LaRC) have led fundamental research and development of an additive manufacturing technology for metallic aerospace structures called Electron Beam Freeform Fabrication (EBF^3). EBF^3 is a NASA-patented[1-3] process to build complex, near-net-shape parts requiring substantially less raw material and finish machining than traditional manufacturing methods. NASA's vision for EBF^3 is first, to enable the manufacture of next-generation metallic aerostructures with improved performance, lower cost and reduced environmental impact; and second, to produce on-demand spare parts, tools, or structural elements for onsite repairs for future long-duration space missions. These parts span a wide range of scale and material choices ranging from small, detailed aluminum parts to large, near-net-shape superalloy components for rocket motors.

The EBF^3 team at NASA LaRC is committed to leading the technology push with continued process improvements. Broader industrial adoption of all additive manufacturing technologies, including EBF^3, will depend on repeatability, inspectability, repairability and process certification. These considerations currently limit the broader industrial adoption of all additive manufacturing technologies, including EBF^3. Optical and thermal sensor-based image acquisition and analysis can address most of these needs.

This paper highlights past efforts and recent progress in the implementation of near-infrared (NIR) imaging to provide thermal and spatial measurements that can be used in a closed-loop control system, enabling automatic, real-time adjustments to maintain consistent thermal and geometric conditions throughout the build cycle. Additional information in the thermal images is used to assess build quality by detecting flaws in prior layers of the deposit.

* karen.m.taminger@nasa.gov; phone 1-757-864-3131; fax 1-757-864-7893; http://www.nasa.gov/langley

2. EBF^3 ADDITIVE MANUFACTURING PROCESS

NASA LaRC presently has a total of three EBF^3 systems: the original machine based upon a commercially available 42kW Sciaky electron beam welder, and two custom-built "portable" systems designed for EBF^3 flight experiments on the NASA C-9 microgravity research aircraft. Figure 1 shows the interiors of the processing chambers of each of the three EBF^3 machines at LaRC. For relative size comparison, the working volume (i.e., volume accessible by both the electron beam and wire feeder) of the large Sciaky machine is approximately 0.75 x 1 x 2 m, while the two portable machines each have working volumes of about 0.3 m^3. The large machine accepts wire spools containing up to about 15 kg of material, while the smaller machines use standard 0.5 kg wire spools. The large system weighs approximately 50,000 kg, while the portable systems each weigh about 900 kg ready to operate.

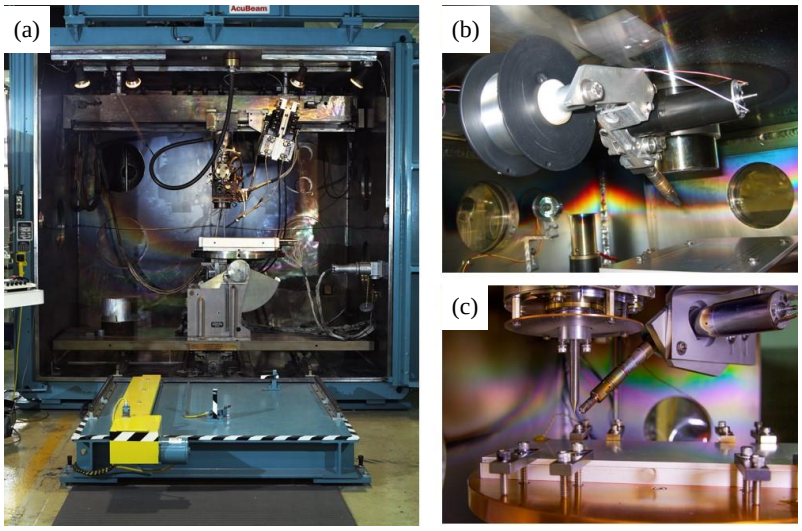

Figure 1. Interior photographs of : (a) large EBF^3 system based on Sciaky electron beam welder; (b) first generation portable EBF^3 system; and (c) second generation portable EBF^3 system.

The operational concept of EBF^3 is to build a near-net-shape metal part directly from a Computer-Aided Design (CAD) file in a layer-additive manner without the need for molds or tooling dies. In this process, an electron beam is used as a heat source to create a small molten pool on a substrate into which wire is fed. The substrate (baseplate) can be composed of identical or different material than the deposited metal depending upon the application. The electron beam and wire feed assembly are translated with respect to the baseplate to follow a predetermined tool path, similar to conventional computer-aided machining practice. The deposited material solidifies immediately after the electron beam has passed, having sufficient structural strength to support itself. This process is repeated in a layer-wise fashion, resulting in a near-net-shape part requiring minimal finish machining. Careful attention to process control is required to minimize transient thermal effects, such as distortion, until the part cools and the part can be removed from the vacuum chamber.

EBF^3 offers several unique attributes among the competing metallic additive manufacturing approaches. First, it is scalable in size and deposition rate, allowing fabrication of parts measuring a few cm^3 up to parts 1 m^3 or larger, restricted only by the size of the vacuum chamber. High deposition rates with larger bead sizes enable near-net-shape construction of large structures using established aerospace alloys such as aluminum 2219 and 6061, stainless steel 304 and 316, Inconel® 625 and 718, and titanium Ti-6Al-4V. Second, it uses wire feedstock as opposed to metal powder for high feedstock usage efficiencies and safe operability in reduced gravity environments such as low-Earth orbit. Third, the electron beam used to melt the metal wire requires that the process be conducted in a vacuum chamber; vacuum enables processing of traditional aerospace alloys, most of which cannot be melted in air without oxidation degrading their metallurgical properties. Finally, EBF^3 offers the promise of fabrication of structures with functionally graded metallurgy. By selectively introducing wires of different compositions during the deposition process, the chemistry and resulting physical properties of the metal structure can be varied continuously throughout the part and tailored to its exact service requirements. Functional grading is currently impractical or impossible for most materials and structures using conventional fabrication methods, but relatively straightforward using EBF^3.

3. CHALLENGES FOR REAL-TIME SENSORS IN EBF^3

While the basic operational concept of EBF^3 is simple, a closer look reveals dozens of variables, each affecting the outcome and many of which are interdependent. There are at least seven major challenges to the acquisition and use of real-time sensor data to monitor and control the process. Past and current imaging techniques and data analyses are underway to detect anomalies and refine the EBF^3 process through real-time monitoring and control to mitigate these challenges.

The first major challenge to sensor integration into the EBF^3 process is the deposition environment itself. Efficient generation and transmission of the electron beam requires high vacuum (10^{-5} Torr or lower), meaning that sensor electronics in the chamber must (preferably) be vacuum-rated. This implies little or no permissible outgassing from electronics or packaging and the ability to run uncooled or with conductive and radiative cooling only. Unlike vacuum processes such as electron microscopy, EBF^3 is a relatively "dirty" process that results in metal vapor contamination of line-of-sight surfaces inside the vacuum chamber. Unprotected optical surfaces such as lenses or mirrors will become coated with metal vapor that will periodically need to be removed. Translation of the part and/or electron beam gun during part fabrication results in a moving molten pool that is difficult to track unless sensors are incorporated into the electron beam gun carriage. The size of the electron beam gun and the gun-to-work distance also place practical limits on the size and placement of cameras or other sensors.

Second, EBF^3 is an inherently thermally transient process. Several factors contribute to this, beginning with its layer-additive nature. The continuously moving molten pool over a relatively cold baseplate or previous layer encounters a different cooling path and thermal mass with each successive layer. Variations in the geometry of the part such as section thickness changes, ends or corners also contribute to these changes. Thermal transients need to be better managed to enable repeatability necessary for certification of additive manufacturing processes for use in many applications. Therefore, sensors capable of measuring thermal distributions are important for tracking changes in the molten pool (by detecting the thermal gradients between liquid and solid phases) over time.

Third, the physical properties of each metal alloy (e.g., specific heat, melting temperature, thermal conductivity, vapor pressure) necessitate different process parameters such as beam power, wire feed rate and translation speed. Factors of 2x-10x difference depending upon the material and part geometry are not uncommon, often requiring equally wideband sensors. Less obvious are process accommodations arising from material properties such as molten pool surface tension and liquid metal viscosity, which affect the shape and behavior of the molten pool during deposition. Differing vapor pressures of various alloying additions can result in selective de-alloying (constituent loss) in the deposited material. Controlling the temperature of the EBF^3 process has been shown to impact alloy compositional losses.[4] The temperature-dependent variation of emissivity also comes into play for thermal imaging, requiring unique sensor calibrations and camera settings to optimize the imaging. While emissivity is well documented for many pure metals and common engineering alloys, it is not generally known for functionally graded materials deposited with EBF^3. Since it is of interest to use EBF^3 to deposit materials with widely varying physical properties, wideband sensors capable of detecting the thermal environment for low melting temperature alloys like aluminum up to high melting temperature alloys like nickel are more versatile.

The fourth challenge involves geometric variations in the deposit that result from imperfect coordination of heat and mass flow (electron beam power and wire feed) during starts, stops and abrupt changes in build direction. These variations include bulbs (build-up of excess material at starts), necking (narrowing of the deposit) or tailing-off (deficit in deposit height approaching a stop). Although bead widths are affected with each of these variations, the more significant impact is on the height of the deposited material. Since the EBF^3 process is a layer-additive process, even minute perturbations in height will accumulate into large errors over time as the build progresses. Even parts measuring as small as 10 cm in height can represent over 100 layers. Therefore, the sensor type and its location in the build chamber must enable precise measurement of the bead height.

The closely related fifth challenge adds consideration of the relative direction of wire in-feed and deposit direction to the geometric variations in the deposit. Changes in the wire orientation with respect to the translation direction (e.g., wire lagging or pushing the molten pool, or entering from the side) and wire elevation (e.g., entry angle relative to the horizontal) can subtly change the geometry of the deposit. Equally important, many practical parts require multiple side-by-side beads to develop the required section width, and the shape of the molten pool depends upon the presence and relative location of

adjacent beads. For example, for multi-bead deposits, it is often easier to "push into" adjacent beads than to reach over them but this is not always possible due to other constraints. If the width of the bead and the influence of the wire on the molten pool can be measured in real-time, minor adjustments to processing parameters such as wire feed rate and translation speed can be implemented to improve part precision.

Sixth, random process errors result from variability in the wire feed. The wire is primarily at room temperature until it crosses into the electron beam path, at which point it is subjected to an abrupt thermal gradient, melting over a very short distance as it enters the molten pool. Larger diameter wire, therefore, retains substantial stiffness as it enters the molten pool, resulting in several errors. In the event of excess heat, insufficient wire feed, or wire feeding above the electron beam/substrate intersection point, dripping occurs. Conversely, insufficient heat, excess wire feed, or wire feeding below the electron beam/substrate intersection point results in wire stabbing which can cause the wire to oscillate back and forth in the molten pool; skip, causing fluctuations in the deposit height; or deflect off the bottom of the molten pool and divert out of the beam altogether. Improper wire location or poor timing of the start/stop sequence will often result in wire sticks. Some errors of this nature have also been observed due to cast (residual curvature or twist in the wire not removed by the wire straightener) or simple mechanical misalignment of the wire feed apparatus that was not immediately apparent. To measure wire feed anomalies, the most important feature to track is the wire position relative to the molten pool. This requires a sensor with a wider field of view and ability to measure geometric features that have widely different temperatures.

The seventh and final major challenge is encapsulation of flaws within the EBF^3 deposits. Voids and porosity have been observed due to contamination (cleanliness) of the wire, wire variability, or programming errors in the steps between side-by-side beads and layers. Inclusions can occur when the molten pool picks up a contaminant from contaminated wire or from metal vapor condensate flaking off and falling into the deposit. Lack of fusion between layers can occur due to insufficient heating before or during the deposition steps, improper programming of the layer height, or oxidized surfaces when the part has been exposed to air prior to initiating or resuming interrupted EBF^3 deposition. Just as observed in welding operations, hot cracking or quench cracking can occur due to high thermal gradients, insufficient preheat or microsegregation that occurs with rapid cooling. Material property variations can also occur due to microstructural or chemical variations. For example, some alloys will form strong textural orientation due to preferential crystallographic freezing that follows the cooling path. Finally, large thermal gradients and thermal contraction can result in residual stresses that will manifest as distortion, or in the extreme case, cracking. These defects and the mechanisms to control and avoid their formation are somewhat understood. The ultimate success and commercial adoption of the EBF^3 technology in many areas may depend upon the ability to detect, quantify and repair flaws that occur during the deposition process. Evaluating thermal diffusivity using thermal imaging cameras is one approach that may enable embedded flaw detection during deposition.[5] However, real-time, in situ flaw detection and assessment may drive development of additional sensors.

4. EBF^3 IMAGING SENSOR IMPLEMENTATIONS

The solution to these challenges resides in integration of imaging systems into the EBF^3 systems to monitor the process. Image analyses to identify the anomalies and control logic to implement corrective action are then required to fully close the processing control loop. Five different imaging hardware approaches have been evaluated in NASA's EBF^3 systems over the past decade. Image analysis and control loop logic are on-going.

4.1 Internal Mount CMOS Camera

Initial NIR imaging approaches to monitoring the molten pool during the EBF^3 process were investigated from 2003 to 2005. The first camera selected was from Silicon Imaging, model SI-1280. This is a 12-bit, digital Complementary Metal-Oxide Semiconductor (CMOS) camera, which has particular advantages for the EBF^3 process environment. Data are digitized in the camera reducing the susceptibility of signals to noise in transmission lines. CMOS cameras directly measure the current in the detector so there is no charge build-up in the pixel wells as in a Charged Coupled Device (CCD). Therefore, CMOS cameras will not bloom or streak when overexposed. For example, if the electron beam energy density is too high, the resulting plasma would "wash out" a normal CCD camera, preventing viewing of the molten pool. A CMOS sensor will simply "peg out" a pixel at its maximum value, leaving adjacent pixels unaffected. The exposure was controlled through a LabView Camera Link interface. This camera has a 1.28 megapixel chip, but can be operated with a smaller region of interest at very high speeds. At 100x100 pixels, frame rates of 3000 fps can be achieved.

The CMOS camera consumes very low power, producing less heat and reducing the need for cooling in the vacuum environment. A water-cooled coldplate was installed against the camera body for precautionary measures, but the camera also operated for short periods of time without overheating in the vacuum environment without the coldplate. The compact design of this camera (45 x 52 x 50 mm) enabled installation on a bracket directly on the electron beam gun. Pinhole and secondary optics were installed with a flow controller to meter argon into the camera/pinhole system to protect the optics from being occluded by metal vapor. This optical camera was bandpass filtered down to the NIR range and calibrated to provide thermal information. Figure 2 shows data from the Silicon Imaging camera on Ti-6Al-4V. The color scale in Figures 2a and 2b was calibrated to show the Ti-6Al-4V liquidus temperature as light orange, and the solidus temperature as blue. The camera was installed in two different locations attached to the electron beam gun: orthogonal to the wire feeder with a wider field of view to capture height and cooling path data (Figure 2a), and opposite the wire feeder focused down on the molten pool to capture molten pool shape and size (Figure 2b). A series of experiments on Ti-6Al-4V was performed, depositing five successive layers on a deposit 25 cm in length, and a single bead width. The solidus temperature was outlined based on analysis of the thermal images. After five layers, the length of the molten zone doubled at constant power and travel speed, illustrating the dependence of the process on geometry and thermal history (Figure 2c). The goal in using these data is to adjust process parameters to maintain a constant tail length and thus cooling rate.

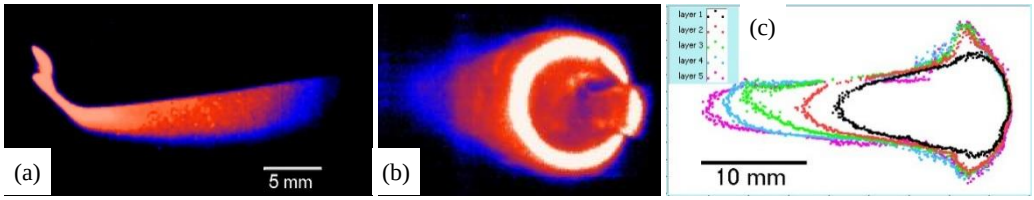

Figure 2. Images from SI-1280 CMOS camera. (a) NIR image from side-mounted orientation. (b) NIR image from top-mounted orientation. (c) Thermal molten pool data from 5 sequential layers showing thermal transients.

4.2 Fiber Optic + External Mount CCD Camera

Although the CMOS camera had high speed data acquisition, good compatibility with the vacuum environment, and resistance to blooming of oversaturated pixels to adjacent pixels, the resolution and low light capabilities were inferior to CCD cameras in the 2003 to 2005 time period. For comparison, the second camera evaluated at that time was a Hamamatsu C8484-05 12-bit CCD with a 1.37 megapixel chip. The CCD camera had excellent NIR characteristics and could operate at low light levels. This camera was also programmed through the LabView Camera Link interface.

The Hamamatsu camera was too large to mount on the electron beam gun and was not well adapted to the vacuum environment. Thus, this set-up relied on fiber optic transmission of the image with a Schott wound image bundle. The fiber bundle passed out of the vacuum chamber to a relay lens and beam splitter, and the image was monitored by two cameras, a Silicon Imaging SI-1280 and a Hamamatsu C8484-05. Each camera had its own relay lens, so magnifications could be independently adjusted. The optical/NIR filters were accessible without opening the vacuum chamber. This setup is shown in Figure 3. The coherent fiber bundle from Schott has transmission out to 1.2 microns (the IR limit of the imaging sensors) and about 800,000 fibers (or pixels). This configuration offered flexibility for process diagnostics. For example, the SI-1280 could be run at very high frame rate for real-time process sensing, and the Hamamatsu run at a slower frame rate with a larger field of view for spatial resolution in the process area and detection of the wire feed position. Filters were used to monitor in the NIR range with the CCD camera, and very short shutter speeds were used to control the high intensity light emanating from the molten pool. This provided thermal details in the molten pool (Figure 3c), but due to the short shutter speed and losses from the fiber optic bundle, thermal data in the surrounding areas were lost. The camera

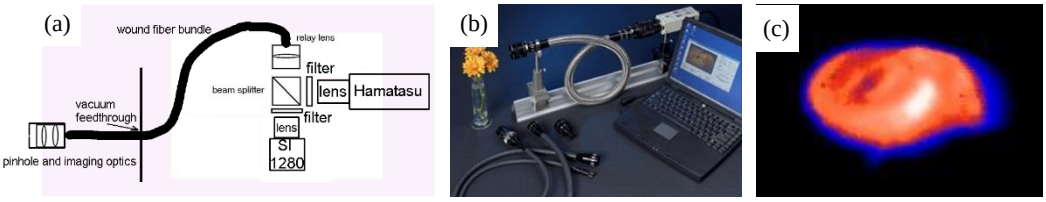

Figure 3. Set-up and images from Hamamatsu CCD camera. (a) Schematic of installation in EBF^3 system. (b) Bench set-up with Schott fiber optics and Hamamatsu camera. (c) NIR image from top-mounted orientation.

was not permanently integrated due to damage sustained to the Schott fiber optic bundle, as a result of fibers shifting with the moving electron beam gun and vacuum. The ends of the fiber optic bundle could be redressed, but was not pursued.

4.3 Backscattered Electron (BSE) Detector

From mid-2008 to mid-2009 an effort was made to develop an electron imaging system that could be used to actively monitor and measure the EBF^3 deposit height and wire position relative to the beam. Additional objectives of this work were to explore the capabilities of the electron beam gun system to raster the beam at relatively high frequency in specific patterns to preferentially direct energy to the wire or the molten pool,[3] and to detect the onset of process errors due to wire feed errors or misalignment.

Normal operation of the EBF^3 electron beam generates large quantities of primary electrons, secondary electrons, x-rays, neutral particles, ions and backscattered electrons, all with a wide range of energies. Of these possible signal sources, backscattered electrons (BSEs) were chosen because of their directionality and high retained energy fraction. A custom-built BSE detector was purchased from ETP-Semra in Australia and installed in the large EBF^3 vacuum chamber. In order to improve the signal-to-noise ratio (i.e., to capture only those scattered from the molten pool), a series of negatively-biased screening electrodes were placed at the entrance to the detector. BSEs of sufficient energy to transit the screening stages enter the detector and strike a phosphor screen, generating photons which travel through a light pipe to a photomultiplier tube. Output from the photomultiplier tube is then used to construct an image of the target area.

Several different mounting arrangements for the detector were tried with varying degrees of success for producing an unobstructed view of the EBF^3 process zone without exposing the sensor to metal vapor. The best viewing angle was ultimately obtained with the detector mounted directly in line with the wire feed nozzle at an elevation angle of about 15° above the workpiece. As with the optical/NIR cameras, the sensor was also susceptible to metal vapor contamination.

Figure 4 shows some high quality images obtained with the BSE detector; however, these images were obtained with very low beam current (1-5 mA) and a raster scan pattern specifically designed for imaging, not deposition. In other words, images of this type could not be obtained using the beam parameters in real time during an actual build; imaging scans would have to be conducted separate from the build process. Also, during the build process, the beam path is confined to the molten pool and not rastered outside a very small target area. It was possible to infer, but not directly measure, the deposit height with a single BSE detector. The efforts to monitor wire position and preferentially direct beam energy into the wire or the molten pool with the BSE detector were quite successful, and revealed that some information as to geometric error conditions (dripping, wire feeding off-center to the molten pool) could easily be detected.

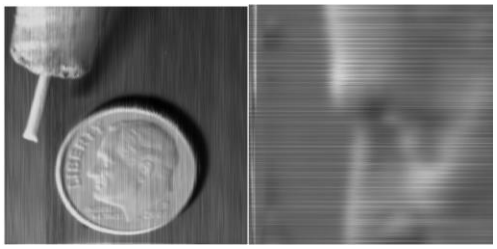

Figure 4. Images from BSE detector using a low power scanned electron beam in the EBF^3 system showing the imaging resolution possible with this detector.

Despite these promising results, BSE imaging was ultimately abandoned as a means to provide information to the closed-loop control system. This was mainly due to its relatively high cost and the bulkiness of the detector system. In addition, the BSE detector required modification of the electron beam rastering and focusing coils to coordinate the beam location with the sensors in the detector. As a research and development tool, the BSE detector was useful, but challenges with obtaining images during beam power and raster patterns typical for deposition, and the ability to image but not measure temperatures led to the decision to explore other sensors.

4.4 Internal Mount CCD Camera

It was learned from the experiences described in sections 4.1 to 4.3 that camera location is critical for observation of the molten pool sufficient to provide data usable for closed-loop control of the process. In 2010, trials were started with

another miniature CCD camera, the Prosilica GC1380H. In order to optimize the image and provide future additional capabilities, an instrumentation ring was designed and attached to the electron beam gun. This mounting arrangement, presented in Figure 5, remains in use today. The instrumentation ring provides the ability to position cameras and other hardware in nearly any location around the gun. The instrumentation ring consists of an upper and lower ring with diagonal struts connecting the upper and lower rings. The cameras (or other instrumentation) are attached to the diagonal struts with sliding brackets. The diagonal struts allow the cameras to be moved to any position around the electron beam gun. The slide brackets allow the pitch angle of the camera to be modified. Currently, trials are underway using two cameras to image the melt pool at 180° and 90° from the wire feeder.

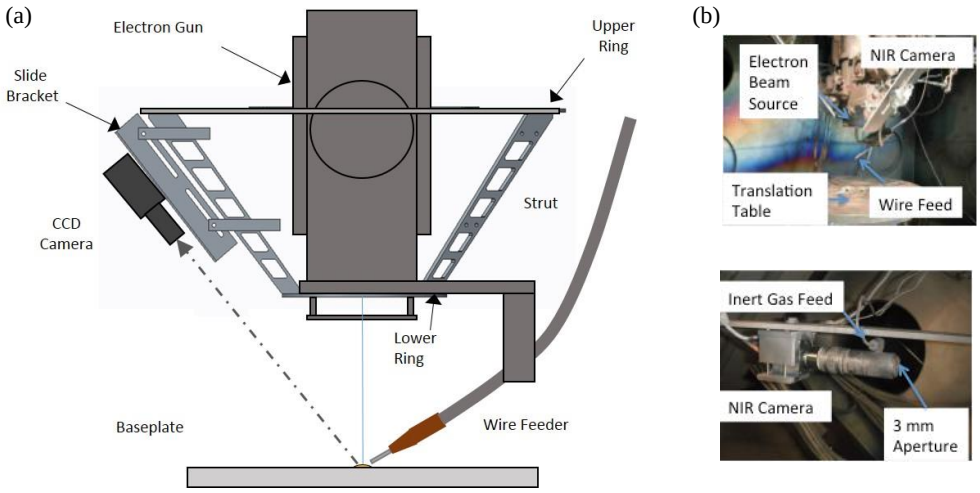

Figure 5. (a) Schematic diagram of CCD camera mounting ring and optical path in EBF[3] system. (b) Photos of NIR camera and gas shield installation in the EBF[3] system.

The NIR band was selected to image metals of higher melting temperatures such as 316 stainless steel, Ti-6Al-4V, and Inconel® 625. The Prosilica GC1380H is a non-cooled CCD camera with a frame rate of 30 Hz at full resolution through a GigE interface. A water-cooled coldplate was installed against the camera body to provide some cooling in the vacuum environment. The camera pixel array size is 1360x1024 (pixel pitch size of 6.45 µm x 6.45 µm). The camera's dynamic range is 12 bits. The imaging spectral band is set at .875 to 1.05 µm using a long pass filter and this allowed imaging temperatures from 700 to approximately 2,200° C. A NIR neutral density filter is used to reduce the transmission by a factor of 10. The C-mount optical package contains a 150-mm relay lens pair, a protective window (B270 material), and an extension tube with a gas fitting. The gas fitting allows for a small amount of inert gas to flow out of the 3 mm diameter aperture and thus prevent window clouding due to residual metallic particles dispersed during the electron beam excitation. Camera resolution is approximately 0.006 cm/pixel. A photograph of the NIR camera installation is shown in Figure 5b.

A radiometric calibration is vital to convert the pixel values (intensity counts) to temperature, define the temperature imaging limits of the system, determine the optimal threshold values for closed-loop control metrics (based on the wire melting temperature), correct for material dependent emissivity, and selection of the optimal integration time. A radiometric characterization was performed on the NIR camera/optic using a calibrated blackbody radiation source set at various temperatures.[5-7] The process involves the calibration of the radiance counts to actual temperature values. The temperature values used were 700, 800, 900, 1,000 and 1,100°C at specified sensor integration times ranging from 10 to 50,000 µs. Using a given emissivity value, the radiance is then converted to temperature using a linear interpolation of the system's radiance response.

Shown in Figure 6 are NIR temperature images and line plots along the deposition of 316 stainless steel (Figure 6a), Ti-6Al-4V (Figure 6b), and Inconel® 625 (Figure 6c). The 316 stainless steel[8] temperature image was obtained using an integration time of 1500 µs and emissivity literature value[8] of 0.66. The Ti-6Al-4V[9] temperature image was obtained using an integration time of 1000 µs and emissivity of 0.48 and the Inconel® 625[10] temperature images were obtained using an integration time of 1500 µs and emissivity of 0.77. The measured temperature values agree with literature values for 316 stainless steel, Ti-6Al-4V, and Inconel® 625 at the transition point for the respective melting point ranges of 1370 to

1400°C, 1604 to 1660°C, and 1290 to 1350°C, respectively.[11-13] This allowed measurement of the molten pool shape and area, the semi-solid area and length, and transient cool down regions. These metrics were used for adjusting process parameters such as beam power, wire feed rate and traverse speed during closed-loop control.

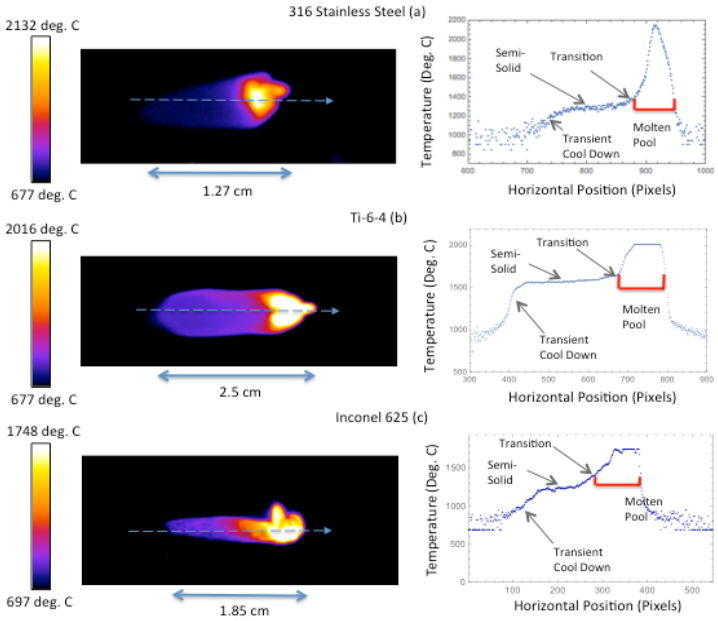

Figure 6. Thermal images of (a) 316 stainless steel, (b) Ti-6Al-4V, and (c) Inconel® 625, with line plots showing the deposition temperature variation.

4.5 Internal Mount Short-wave IR (SWIR) Camera

An interest in imaging lower melting temperature alloys like aluminum led to examination of longer wavelength cameras. In 2015, a Short-wave Infrared (SWIR) camera was installed in the portable EBF^3 system. The portable EBF^3 system has a more compact design. Due to the space limitations, a periscope-style camera assembly was developed in order to image the molten pool. The mechanical and optical arrangements are illustrated in Figure 7. The electron beam gun's robotic arm has four degrees of freedom in this system. The camera is attached to the front side of the robotic arm in a vertical position which does not limit the system's range of motion. Mirrors are then used to direct the image to the camera. The SWIR camera is also actively cooled by a coldplate which is plumbed to an external water chiller. The SWIR camera is positioned approximately 45° off the forward deposition direction (the direction to the left in Figure 7a). Two mirrors direct the image to the camera. Due to the space limitations, the system's wire feeder is positioned approximately 45° off the opposite side of the robotic arm (immediately behind the camera in Figure 7a).

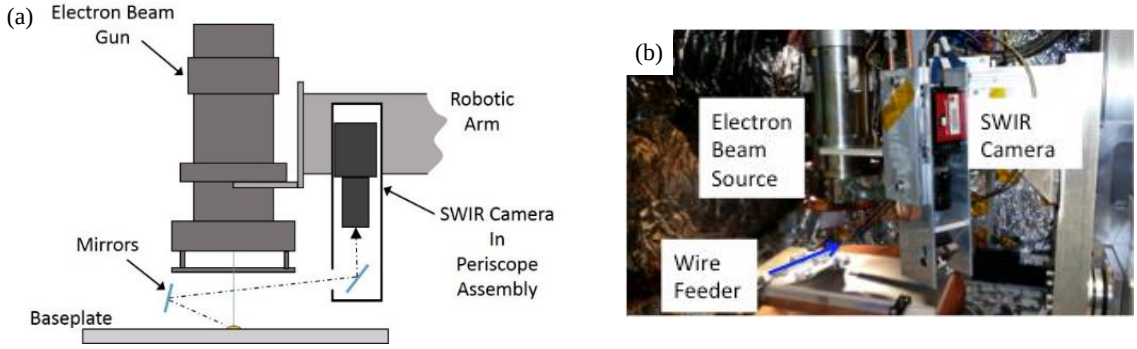

Figure 7. (a) Schematic diagram of SWIR camera mounting and optical path in the portable EBF^3 chamber. Wire feeder is mounted directly behind the camera assembly (not illustrated). (b) SWIR camera and periscope installation in the portable EBF^3 chamber.

The SWIR band is required to image metals of lower melting temperatures such as aluminum. The digital SWIR camera used is the Allied Goldeye G-032. This camera requires temperature stabilization using an internal thermoelectric cooler. The camera pixel array size is 636x508 (pixel pitch size of 25 µm x 25 µm). The camera's dynamic range is 14 bits with a maximum frame rate of 100 Hz at full resolution through a GigE interface. The spectral response of the camera's detector is approximately .950 – 1.7 µm and this allowed measurement of temperatures from 300 to around a 1000°C. The camera is protected within an aluminum enclosure that is liquid cooled. The camera's optic used is a C-mount 50 mm lens with 75% or better transmission between .700 to 1.9 µm. A protective window using a Mylar polyester film is used to protect the optical system from metal vapor resulting from the electron beam deposition process. Camera resolution is approximately 0.015 cm/pixel. With a molten pool size of 0.2 to 0.6 cm, this camera resolution results in the regions of interest being captured by 10's of pixels across.

Similar to the NIR camera calibration, a radiometric characterization was performed using a calibrated blackbody radiation source set at various temperatures for the SWIR camera. The process involves the calibration of the radiance counts to actual temperature values. The temperature values used were 300, 400, 500, 550, and 600°C at specified sensor integration times ranging from 120 to 15,000 µs. Shown in Figure 8 is the SWIR temperature image and line plot collected during the deposition of aluminum 2219. The aluminum 2219[14] temperature image was obtained using an integration time of 200 µs and emissivity value of 0.2. As shown on the line plot, the measured temperature values agree with aluminum 2219 literature values[15] at the transition point for the melting point range of 543 to 643°C. This allowed measurement of the molten pool shape and area, but the semi-solid and transient cool down regions were not detected for the integration time and frame rate (20 Hz) used. This was expected due to the high thermal conductivity of aluminum. These initial results are still under investigation, and further experiments are planned.

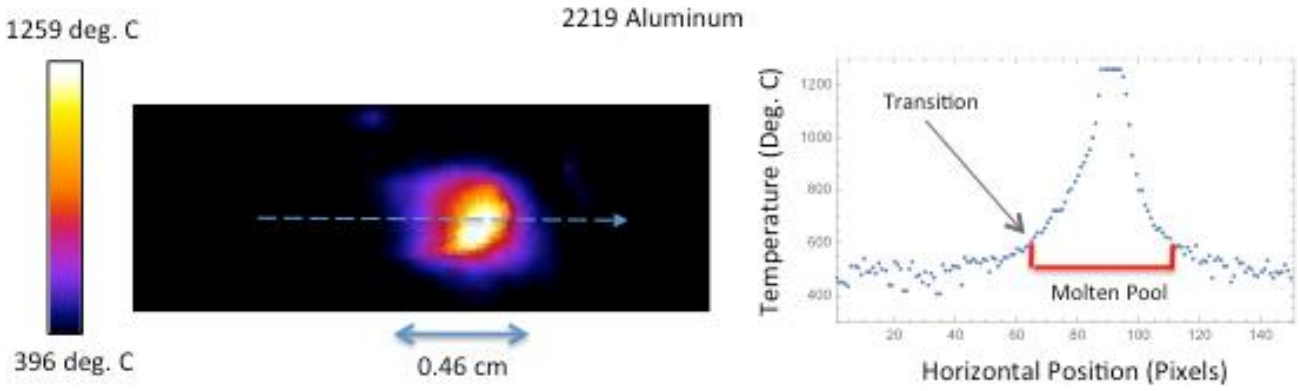

Figure 8. SWIR temperature image and line plot during EBF[3] deposition of aluminum 2219.

5. DISCUSSION

The vacuum, thermal, metal vapor environment and limited space in the EBF[3] process pose some challenges for sensors selection and integration into the system for real-time process monitoring and feedback. Early in the development of EBF[3], it was recognized that sensor data were necessary to understand the nature of process anomalies and introduction of flaws into the final components. Since EBF[3] is inherently a thermally transient process, thermal data were also of interest to correlate with microstructural and non-destructive evaluations to identify metallurgical features and flaws that drive the mechanical properties of the deposited materials. Due to space constraints, multiple sensors may not be feasible, so sensors that can capture all of the suitable data are sought. This work has also highlighted the need to consider a variety of factors in determining the suitability of a particular imaging technology for use in the EBF[3] process. Suitability is determined by consideration of the available frame rate, resolution, signal-to-noise ratio, spectral response, vacuum compatibility, ruggedness, size, and cost. Table 1 summarizes qualitatively how well the five sensors captured data to address the EBF[3] process challenges identified.

Table 1. Summary of sensor suitability to measure features of interest associated with EBF³ process challenges.

Sensor Technology / EBF³ Process Challenges	Section 4.1: Internal Mount CMOS Camera	Section 4.2: Fiber Optic + External Mount CCD Camera	Section 4.3: Internal Mount Backscattered Electron (BSE) Detector	Section 4.4: Internal Mount CCD Camera	Section 4.5: Internal Mount SWIR Camera
1) **Deposition environment** (vapor contamination; vacuum compatibility)	Pinhole optics; Cold plate for camera cooling	Pinhole w/ fiber optics; Externally mounted	Vapor shield; Fully vacuum compatible	Pinhole optics; Cold plate for camera cooling	Pinhole optics; Cold plate for camera cooling
2) **Thermal transients**	Yes	Limited	No	Yes	Yes
3) **Alloy physical properties/melting range**	NIR signature	NIR signature	n/a	NIR signature	SWIR signature
4) **Height measurement** (with one camera)	Limited	Limited	Not demonstrated	Limited	Limited
5) **Width measurement**	Yes	Limited	Yes, but not demonstrated in real time	Yes	Limited
6) **Wire/molten pool tracking**	Yes	Limited	Not demonstrated	Yes	Limited
7) **Real-time flaw detection**	Yes	Limited	Limited	Yes	Yes

6. CONCLUDING REMARKS

The past 15 years of research and development of EBF³ at NASA Langley have highlighted many challenges to obtaining a consistent, repeatable process. These challenges include: deposition environment, thermal transients, alloy physical properties/melting range, height measurement, width measurement, wire/molten pool tracking, and real-time flaw detection. Although EBF³ is a challenging environment in which to capture data, it is also a signal-rich environment with metal vapor, plasma, acoustic emissions, photons, electrons, x-rays, neutral particles, ions and backscattered electrons, all with a wide range of energies. Selection and integration of sensors into the EBF³ system is key to understanding and quantifying resulting features during the deposition process, leading towards fully-integrated closed-loop process control.

To date, the focus has been on imaging sensors: internally-mounted CMOS, CCD, BSE and SWIR detectors, and a fiber optic-transmitted signal to an externally-mounted CCD camera. Each approach has provided useful data. The internally-mounted CMOS, CCD and SWIR cameras have provided wider field of view and thermal images of value to monitoring many of the challenges associated with the EBF³ process. The fiber optic-transmission to the externally-mounted CCD camera had advantages in keeping the camera outside of the vacuum chamber, but damage to the fiber optic bundle truncated this effort early. Likewise, difficulty with the size and cost of the BSE detector, and the inability to obtain thermal information, led to the decision to discontinue efforts with the BSE detector. Both techniques that were abandoned showed some promise, but implementation issues favored adopting approaches with the internal mounting of smaller, inexpensive NIR sensors. The SWIR camera, although expensive, is the only one able to measure lower temperatures of interest for aluminum alloys.

Closed-loop control of the EBF³ process for higher melting temperature alloys like Ti-6Al-4V and Inconel® 625 has been successfully implemented using the internally-mounted CMOS and CCD cameras. As work on the closed-loop control system continues, expanding the temperature range to include lower melting temperature alloys like aluminum is of interest, as well as refining the data capture and analyses to enable better thermal control and mitigation approaches to

address the challenges identified. The first step in obtaining actionable data has been achieved with the NIR and SWIR cameras. The next step is developing the algorithms to identify the signatures related to each challenge, and building the logic into the closed-loop control system to refine the process through continuous, real-time monitoring and feedback.

Looking beyond continuing refinements of closed-loop process control, the next technological goal that will significantly advance the state of the art in EBF^3 (and perhaps all metal additive manufacturing technologies) may be real-time nondestructive inspection acceptable for process and part certification. Work has already been initiated to use the same NIR and SWIR sensors to measure the EBF^3 molten pool and detect embedded flaws within the process. Connecting these data to the non-destructive evaluation results taken after deposition is the future goal towards obtaining a repeatable, certifiable process.

REFERENCES

[1] Taminger, K. M. B., Watson, J. K., Hafley, R. A., and Petersen, D. D., "Solid Freeform Fabrication Apparatus and Method," US Patent # 7,168,935, 2007.

[2] Taminger, K. M. B., Hofmeister, W., and Hafley, R. A., "Use of Beam Deflection to Control Electron Beam Wire Deposition Processes," US Patent # 8,344,281, 2013.

[3] Taminger, K. M. B., Hafley, R. A., Martin, R. E., Hofmeister, W., and Seufzer, W., "Closed Loop Process Control for Electron Beam Freeform Fabrication and Deposition Processes," US Patent # 8,452,073, 2013.

[4] Sankaran, S. N., Sinden-Redding, M. R., Frazier, W. E., Hafley, R. A., Lach, C. L., and Taminger, K. M., "An Understanding of Al Loss During EBF^3 Deposition of Ti-6Al-4V Alloys from Cross-sectional Geometry and Microanalysis," 2010 AeroMat Conference, 22 June, 2010, Bellevue, WA.

[5] Zalameda, J. N., Burke, E. R., Hafley, R. A., Taminger, K. M., Domack, C. S., Brewer, A. and Martin, R. E., "Thermal Imaging for Assessment of Electron-Beam Freeform Fabrication (EBF^3) Additive Manufacturing Deposit," *Proc. SPIE* 8705, Thermosense: Thermal Infrared Applications XXXV, 87050M (May 22, 2013).

[6] Spisz, T. S., Taylor, J. C., Gibson, D. M., Kwame, O. W., Horvath, T. J., Zalameda, J. N., Tomek, D. M., Berger, Tietjen, A. B., Tack, S., and Schwartz, R. J., "Processing Near-Infrared Imagery of Hypersonic Space Shuttle Reentries," Thermosense XXXII Conference at 2010 SPIE Defense, Security, and Sensing Symposium, 5-9 April 2010, Orlando, FL, Paper 7661-17.

[7] Zalameda, J. N., Horvath, T. J., Tomek, D. M., Tietjen, A. B., Gibson, D. M., Taylor, J. C., Tack, S., Bush, B. C., Mercer, C. D., and Shea, E. J., "Application of a Near Infrared Imaging System for Thermographic Imaging of the Space Shuttle during Hypersonic Re-entry," AIAA Paper 2010-245, Jan. 2010.

[8] Emissivity of 316 Stainless Steel, http://www.coleparmer.com/TechLibraryArticle/254, April 2013.

[9] Boivineau, M., Cagran, C., Doytier, D., Eyraud, V., Nadal, M-H., Wilthan, B, and Pottlacher. G., "Thermophysical Properties of Solid and Liquid Ti-6Al-4V (TA6V) Alloy," *International Journal of Thermophysics*, 27, no. 2 (2006), pp. 507-529.

[10] Emissivity of Inconel® 625, http://www.specialmetals.com/assets/documents/alloys/inconel/inconel-alloy-600.pdf, March 2, 2106.

[11] Melting Point of 316 Stainless Steel, http://www.goodfellow.com/E/Stainless-Steel-AISI-316.html, April 2013.

[12] Melting Point of Ti-6Al-4V, http://asm.matweb.com/search/SpecificMaterial.asp?bassnum=MTP641, April 2013.

[13] Melting Point of Inconel® 625, http://asm.matweb.com/search/SpecificMaterial.asp?bassnum=NINC33, March 2, 2016.

[14] Wen, C.D., and Chai, T.Y., "Experimental Investigation of Emissivity of Aluminum Alloys and Application of Multispectral Radiation Thermometry," *Applied Thermal Engineering*, 31 (2011), pp. 2414–2421.

[15] Melting Point 2219 Aluminum, http://asm.matweb.com/search/SpecificMaterial.asp?bassnum=MA2219T62, Feb. 29, 2016.